Manuscript 4685 Revision 1

Further complexities of the 10Å-phase revealed by infrared spectroscopy and X-ray diffraction

Alison R. Pawley[1] and Mark D. Welch[2]

[1]School of Earth, Atmospheric and Environmental Sciences, University of Manchester, Manchester M13 9PL, U.K.

[2]Department of Mineralogy, The Natural History Museum, London SW7 5BD, U.K.

ABSTRACT

Infrared spectroscopy, combined with the results of previous NMR studies, has been used to evaluate the OH and H_2O environments in 10Å-phase ("TAP"), nominally $Mg_3Si_4O_{10}(OH)_2 \cdot H_2O$. Two partially deuterated samples of TAP synthesized under different conditions have very similar IR spectra, indicating that the phase has a reproducible structural state. IR spectra were also collected of samples of fully Ni-substituted and partially deuterated TAP, and of samples heated for 1 – 2 h at 500 °C in order to remove structural H_2O/D_2O and leave behind bands due to OH/OD of the 2:1 layer. A high-pressure study of the Ni-TAP sample confirmed that the behavior of its H_2O and OH/OD bands was analogous to that observed in previous studies of Mg-TAP. Comparison of the IR spectra of unheated, heated and compressed samples has allowed three different types of Mg-OH (Mg-OD) stretching bands to be identified, two of which are further split, indicating subtle complexities in the TAP structure. The third band is identical to the band in talc. Two interlayer H_2O stretching bands have been identified. The presence of an absorption

feature that is broader than these interlayer H_2O bands suggests that there is a second type of more weakly bonded H_2O. On heating to 500 °C, the main interlayer H_2O bands are lost, the talc-like band is unchanged, and shifts in the other Mg-OH band frequencies indicate a change in environment following the loss of the interlayer H_2O. At the same time the signature of a silanol group is possibly revealed from the coincidence of band positions in the Mg-TAP and Ni-TAP spectra. The recognition of three distinct Mg-OH (Ni-OH) environments in Mg-TAP (Ni-TAP) is consistent with the structural model of TAP proposed by Welch et al. (2006) and Phillips et al. (2007), in which the transformation from talc to TAP involves a key change from hydrophobic to hydrophilic character that enables hydration of the interlayer. A final level of complexity is indicated by the identification of a 3*c* trigonal superstructure from single-crystal XRD, implying a structure analogous to that of the 3*T* phengite polytype, with interlayer H_2O fulfilling the role of K. The incorporation of interlayer H_2O through the formation of silanol groups has implications for the amount of water contained in 10-Å phase and related phyllosilicates in the Earth's mantle. Moreover, the reproducibility of the key features of the IR spectra for different samples implies that this water content is fixed.

INTRODUCTION

The 10-Å phase ("TAP"), a high-pressure synthetic phyllosilicate related to talc, has been the subject of numerous experimental studies since the first report of its synthesis by Sclar et al. (1965), due to its potential significance as a host of water in subduction zones. TAP is stable at pressures above 5 GPa, where it forms from the reaction of talc, $Mg_3Si_4O_{10}(OH)_2$, with water (Pawley and Wood 1995). Above 700 °C it breaks down to

47 enstatite + coesite + water (Pawley et al. 2011). Therefore any talc that is carried down into
48 the Earth's mantle in subducting slabs will react to TAP at depths of around 200 km if the
49 temperature remains below 700 °C. Talc forms in subducting slabs from hydration of
50 mantle peridotite (e.g., Evans and Guggenheim 1988). Because of its mechanical weakness
51 and anisotropy, its presence in subduction zones is likely to have a significant effect on
52 rheological and seismic behavior (e.g., Hirauchi et al. 2013). TAP has similar physical
53 properties, and so it too would play an important role in the geophysical properties of
54 subducting slab, as well as delivering water to greater depths than is possible in talc.

55 The most obvious transformation in forming TAP from talc + H_2O is the expansion of
56 the basal spacing as H_2O is incorporated into the interlayer space between the 2:1 layers of
57 talc. However, the amount of H_2O incorporation, and its variability with run conditions,
58 have been difficult to quantify. Attempts to measure the H_2O content have yielded
59 concentrations ranging from 0.65 to 2 H_2O per formula unit of talc (Bauer and Sclar 1981;
60 Wunder and Schreyer 1992; Yamamoto and Akimoto 1977). The structure reported by
61 Comodi et al. (2005) from single-crystal X-ray diffraction contains a single H_2O molecule,
62 which is located at the (000) site of the interlayer. Attempts to use computer simulation (*ab*
63 *initio* methods) to infer the state of hydration assume that TAP is simply a hydrated talc,
64 and have not provided good constraints on the likely H_2O content, let alone plausible
65 structural mechanisms for hydration (e.g., Fumagalli and Stixrude 2007). Furthermore,
66 such studies ignore the problem that talc is hydrophobic.

67 Until recently, no mechanism for the incorporation of stoichiometric amounts of H_2O
68 into TAP had been proposed. However, NMR studies by Welch et al. (2006) and Phillips et
69 al. (2007) provide clear evidence for the presence of Si vacancies in TAP, which must be

70 associated with Si-OH groups. These silanol groups confer a hydrophilic character upon the
71 sheets of tetrahedra, which facilitates the incorporation of interlayer H_2O. The model
72 developed by Phillips et al. (2007) is shown in Figure 1. The presence of vacant Si sites
73 leads to triplets of Si-OH groups around each vacancy, along with a new Mg-OH group (type
74 B) that is topologically distinct from the "normal" talc-like Mg-OH environment (type A).
75 The creation of the Si vacancy also leads to a change in topology of the three nearest talc-
76 like Mg-OH groups (type C). Thus, the model predicts three distinct types of Mg-OH groups
77 in TAP. An H_2O group is hydrogen-bonded to each silanol OH. The hydrophilic tetrahedral
78 sheet in TAP contrasts with the hydrophobic sheet of talc. Hence, when talc transforms to
79 TAP at high pressure, this is due to the formation of Si vacancies, silanols and a resulting
80 hydrophilic structure. The ^{29}Si MAS NMR spectrum of sample DTAP3 reported by Welch et
81 al. (2006) implies approximately 1 in 20 Si vacancies (5%). In talc there are 10 OH for
82 every 20 Si. Therefore in TAP with 1 in 20 Si vacancies, the ratio of A-, B- and C-type Mg-OH
83 and silanols is 7:1:3:3.

84 The structural mechanism for interlayer hydration proposed by Phillips et al. (2007),
85 in which three H_2O groups are associated with each Si vacancy, allows considerable H_2O
86 contents to be achieved with minor vacancy formation. A chemical formula corresponding
87 to TAP with 5% Si vacancies is $Mg_3Si_{3.8}O_{9.2}(OH)_{2.8}\cdot 0.6H_2O$. With 8% Si vacancies, the
88 formula is $Mg_3Si_{3.68}O_{8.72}(OH)_{3.28}(OH)_2\cdot H_2O$. Just 2% Si vacancies (near the analytical
89 uncertainty levels of Si for electron microprobe analysis) allows 0.25 H_2O per formula unit
90 to be incorporated into the TAP structure.

In this paper we report the results of spectroscopic and diffraction experiments on partially deuterated TAP (Mg-TAP) and Ni-substituted TAP (Ni-TAP) that point to new levels of complexity in the structure of this beguilingly simple phase.

EXPERIMENTAL METHODS

Sample synthesis

Synthesis of the Mg-TAP is described in Welch et al. (2006). Samples from two different synthesis experiments were used in the present study. They were synthesized from a mixture of $Mg(OD)_2$ and SiO_2 at 6.5 GPa, 600 °C for 400 h (sample DTAP3) and 150 h (DTAP4). DTAP3 is the same sample as used for ^{29}Si MAS NMR spectroscopy in Welch et al. (2006). The Ni-TAP was synthesized from synthetic Ni-talc [$Ni_3Si_4O_{10}(OH)_2$] + D_2O. The Ni-talc was synthesized hydrothermally from an oxide gel at 0.2 GPa, 500 °C (5 days). The Ni-TAP synthesis experiments used a multi-anvil apparatus at the University of Manchester. Samples were sealed in platinum capsules along with 10 – 15 wt % D_2O. The experimental procedure was the same as described in Welch et al. (2006). At the end of each experiment, capsule integrity was checked by measuring the weight before and after puncturing the capsule and placing in a drying oven for around an hour.

X-ray powder diffraction (XRPD)

All run products were studied by XRPD in order to check purity, identify product phases and to determine unit-cell parameters. The XRPD pattern of sample DTAP3 has already been reported by Welch et al. (2006). In order to minimize the effects of preferred orientation, which can be extreme for phyllosilicates, we prepared small spheres of a few

114 milligrams of powder bound in cow gum and mounted on a glass fibre. We used a Genix
115 microsource X-ray generator equipped with CuKα radiation operated at 45 kV, 40 mA, and
116 an Enraf-Nonius one-dimensional position-sensitive detector. A Gandolfi movement was
117 used to maximize sample averaging and minimize preferred orientation. Samples diffracted
118 out to ~80 °2θ, and preferred orientation effects were minimal.
119
120 **Single-crystal X-ray diffraction (SCXRD)**
121 All Ni-TAP products and sample DTAP4 were too fine-grained for analysis by SCXRD.
122 However, the product of sample DTAP3 contained crystals of Mg-TAP that were large
123 enough. Six crystals were studied. Each was mounted on a non-diffracting amorphous-
124 carbon fibre (0.01 mm diameter), itself attached to a glass fibre base. Data were collected
125 using an XcaliburE four-circle diffractometer equipped with an EoS 1K CCD detector (both
126 Agilent Technologies) and MoKα radiation (50 kV, 45 mA). The data collection strategy was
127 determined from a 30-min pre-experiment. Pure ω scans were used with a scan-width of 1°
128 and frame-time of 60 s. The full data collection lasted 16 h. Unit-cell parameters were
129 obtained using reflections with $I > 7\sigma(I)$. Reflection intensities were corrected for Lorentz-
130 polarization effects and absorption (Multiscan) and converted to structure factors using
131 CrysalisPro (®Agilent Technologies). Structure solution by Direct Methods and structure
132 refinement were carried out using SHELX (Sheldrick 2008) within the WinGX environment
133 (Farrugia 1999).
134

Infrared (IR) spectroscopy

Powder IR spectra were collected using a Perkin Elmer *Spectrum One* FTIR spectrometer at the Natural History Museum. A resolution of 2 cm^{-1} was used, with a scan time of 16 s from 400 – 4000 cm^{-1}. KBr was used as a reference standard. Before collecting the spectra, sample discs and the blank KBr disc were heated at 140 °C for 1 day. A set of spectra was collected for samples DTAP3, DTAP4, and all Ni-TAP samples. Some of the discs were then heated in a muffle furnace to 500 °C for 1 – 2 h, crushed, repressed and their spectra recollected as before. In a separate experiment a new disc of (unheated) DTAP4 was prepared and heated to 600 °C for 3 h and its spectrum collected. In addition, two spectra of sample DTAP3 were obtained using the IR microspectroscopy station at the Synchrotron Radiation Source, Daresbury Laboratory. The station set-up is described in Pawley and Jones (2011). The sample was placed on a BaF_2 disc, and one spectrum collected of a single crystal, the other of a small clump of crystals.

In order to establish if Ni-TAP behaves in a similar way to Mg-TAP, we compressed one of the Ni-TAP samples to 9 GPa. High-pressure synchrotron IR spectra were collected using a diamond-anvil cell at the Swiss Light Source (SLS). Details of the IR procedures and instrumentation used at the SLS are given in Jennings et al. (2010) and Welch et al. (2012). A sample chamber was created by filling the gasket hole (0.2 mm diameter) with dry CsI powder and then pressing a small clump of Ni-TAP powder into it with the top diamond. Pressure was determined using the ruby-fluorescence method (Mao et al. 1986). Two ruby fragments were loaded into the CsI plug along with the Ni-TAP powder.

RESULTS

Ni-TAP synthesis experiments

Four synthesis experiments were carried out using the synthetic Ni-talc + D_2O as starting material. An additional experiment used the Ni-talc gel + D_2O. The experimental conditions and run products are listed in Table 1, together with the conditions for the Mg-TAP synthesis experiments. All Ni-TAP synthesis experiments except NTAP3 showed visible fluid escape on puncturing the capsule after the run. For these four experiments, the amount of D_2O incorporated into the run product, which was the difference in weight between added D_2O and fluid released after puncturing, varied from 6 to 11 wt%. The maximum apparent incorporated D_2O is in the sample that did not transform to 10-Å phase (NTAP4), which means that these concentrations cannot be used to indicate the D_2O content of the run product. It is likely that some D_2O was lost during the capsule loading stage. Experiment NTAP3 showed only a small weight loss after puncturing and drying, suggesting water loss during the experiment.

Experiment NTAP1 suffered a short circuit after running for just 40 min, and NTAP2 also experienced heating problems. Nevertheless, both run products showed 100 % transformation to TAP. After experiment NTAP2, a slight modification was made to the multi-anvil apparatus to keep the anvils apart and prevent another short circuit. Subsequent recalibration of pressure revealed a lower pressure than intended in experiments NTAP3 and NTAP4 (6.2 GPa instead of 6.5 GPa), which has led to the formation of talc. In NTAP4 there is also a minor amount of TAP, which means that the reaction Ni-talc + H_2O = Ni-10-Å phase must occur at close to 6.2 GPa at 600 °C. This is a considerably higher pressure than for the corresponding reaction of Mg-talc to Mg-10-Å

phase (~4.9 GPa at 600 °C, Pawley et al. 2011). Experiment NTAP5 was run at a higher pressure and produced 100% TAP. As well as forming Ni-talc, XRPD of experiment NTAP3 showed the formation of an amphibole whose diffraction pattern most closely matches that of grunerite, implying an amphibole of composition $Ni_7Si_8O_{22}(OH)_2$.

Diffraction patterns of NTAP1 and NTAP4 are compared in Figure 2. The relationship between the talc and TAP structures is clear, with TAP showing an increased basal spacing with respect to talc. Unit-cell parameters of NTAP1 derived from XRPD (Le Bail refinement) are: a = 5.3189(5) Å, b = 9.1797(6) Å, c = 10.068(1) Å, β = 100.33(1)°, V = 483.6(1) Å^3; for NTAP5 they are: a = 5.3310(6) Å, b = 9.174(1) Å, c = 10.110(1) Å, β = 100.39(1)°, V = 486.3(1) Å^3. From a comparison of these parameters with those of DTAP3 measured by Welch et al. (2006) – a = 5.3297(9) Å, b = 9.205(3) Å, c = 10.202(3) Å, β = 100.08(2)°, V = 492.8(2) Å^3 – it can be seen that substitution of Ni for Mg in the TAP structure causes a small reduction in volume, which is mostly seen as a decrease in the basal spacing. The similarity of cell parameters for NTAP1 and NTAP5 suggests that the effect of different run durations (0.7 h for NTAP1 and 97 h for NTAP5) on the state of hydration is minor.

Single-crystal XRD

Six crystals of DTAP3 were examined by SCXRD and all showed the same diffraction behavior, which was characterised by rows of superlattice reflections associated with a 3c superstructure. However, strong modulated diffuse scattering is superimposed upon these superlattice reflections, which did not allow their intensities to be integrated satisfactorily (R_{int} = 0.11 – 0.15), although peak positions were accurately determined for refinement of unit-cell parameters. For the best DTAP3 crystal studied, the unit-cell parameters of the

trigonal $3T$ cell are: a = 5.3094(2) Å, c = 30.073(2) Å, V = 734.16(6) Å^3 ($1M \rightarrow 3T$ transformation matrix = ½ -½ 0/½ ½ 0/1 0 3). In terms of the $3T$ cell, rows of superlattice reflections occur for h, $k \neq 3n$, as shown in Figure 3. An attempt to refine the structure in the monoclinic subcell ($C2/m$) confirmed the basic substructure reported by Comodi et al. (2005), but also revealed the presence of a minor second component in difference-Fourier maps that is rotated by 60° relative to the main component. After the SCXRD experiment, the crystal was heated in a muffle furnace to 500 °C for 1 h and studied again. However, the heated crystal did not diffract. It appeared to be delaminated, with obvious cracks and the flaky aspect of a damaged book. We interpret the non-diffracting nature of the heated crystal as being due to substantial loss of interlayer H_2O that removes hydrogen bonding across the interlayer and thereby renders the structure incoherent and effectively two-dimensional, with no periodicity along *c*.

Infrared spectra

IR spectra of Mg-TAP: unheated samples. Powder and single-crystal IR spectra of unheated samples of DTAP3 and DTAP4 are shown in Figure 4, and stretching frequencies are listed in Table 2. The nominally pure D_2O synthesis environment evidently also contained H_2O, so that in addition to well-resolved spectral detail in the OD region, there are strong bands in the OH region. These are less intense in the DTAP4 spectrum than the DTAP3 spectra. The similarity of the powder spectra of DTAP3 and DTAP4 indicates little difference in the structural states of samples synthesised for 150 h (DTAP4) and 400 h (DTAP3). The spectra comprise three pairs of sharp bands at 3675/3665, 3643/3630 and 3588/3577 cm^{-1}, each having an OD counterpart at 2711/2704, 2683/2668 and

226 2645/2626 cm^{-1}, respectively. The ν_{OH}/ν_{OD} wavenumber ratios for these bands range from
227 1.355 to 1.362 and are very close to the theoretical value of 1.374, assuming that O-H and
228 O-D bonds have the same force constant. Another sharp band in the OD region, at 2732 cm^{-1}, with a shoulder at 2751 cm^{-1}, does not at first sight appear to have an OH counterpart.

230 In addition to these sharp bands, there is a broad but well-defined band centred at
231 3268 cm^{-1}, with a corresponding OD band at 2440 cm^{-1}. The wavenumber ratio of this pair
232 of bands is 1.339, which is lower than the values for the sharp bands. Between the set of
233 sharp OH/OD bands and the broader 3628/2440 band is an ill-defined broad feature of
234 variable intensity centred at ~ 3430 cm^{-1}, with a corresponding very weak OD feature
235 centred at ~2555 cm^{-1}.

236 **IR spectra of Ni-TAP: unheated samples.** The powder-IR spectra of NTAP1, 2 and 5
237 (all 100% Ni-TAP) are very similar. Figure 5 shows the spectrum of NTAP5, together with
238 that of NTAP4, which comprises talc + minor TAP. All Ni-TAP spectra consist of four well-
239 defined OH bands at 3672, 3626, 3588 and 3532 cm^{-1}, a sharp OD band at 2676 cm^{-1} and
240 three small bands at 2731, 2648 and 2607 cm^{-1}. The 3626/2676, 3588/2648 and
241 3532/2607 cm^{-1} bands are identified as OH/OD pairs since ν_{OH}/ν_{OD} = 1.355 in each case.
242 Assuming that the 2731 cm^{-1} band is the OD counterpart of the 3672 cm^{-1} band, their
243 ν_{OH}/ν_{OD} = 1.345. In addition to these sharper bands, there is an intense broad band at 3256
244 cm^{-1} that has an OD counterpart at 2440 cm^{-1} (ν_{OH}/ν_{OD} = 1.334). Lastly, as with the DTAP
245 samples, there is an ill-defined broad feature centred at ~ 3430 cm^{-1}. In this case there is no
246 equivalent OD band. The NTAP4 spectrum contains strong sharp bands at 3626 and 2676
247 cm^{-1}, with additional weak bands due to the presence of minor TAP.

IR spectra of Mg-TAP and Ni-TAP: heated samples. Figure 6 shows the unheated DTAP4 spectrum from Figure 4 together with spectra of three different heated discs of DTAP4, two that were heated at 500 °C for 2 h and the third that was heated at 600 °C for 3 h. After heat treatment at 500 °C, DTAP4 retains the OH/OD bands at 3675 and 2711 cm^{-1}. A shoulder is evident on the high-frequency side of these bands, at 3686/2719 cm^{-1}. The other sharp bands from the unheated spectrum are not retained, but instead there is a broader band at 3587/2651 cm^{-1}, with a weak shoulder on the high-frequency side. Again there is an intermediate broad feature of variable intensity. It shows a small shift in frequency from the unheated spectrum, being centred at ~3445 cm^{-1}. Its weaker OD equivalent is at ~2530 cm^{-1}. The 600 °C spectrum is very similar to the 500 °C disc 2 spectrum, except that the shoulder on the high-frequency side of the 2651 cm^{-1} band is resolved into two bands at 2689 and 2677 cm^{-1}, and there is no feature at 2530 cm^{-1}.

After heat treatment at 500 °C for 1 h, NTAP1 retains the sharp OH/OD bands at 3626 and 2676 cm^{-1}, and again, a shoulder is evident on the high-frequency side of these bands, at 3637/2684 cm^{-1} (Fig. 5). The other sharp bands are replaced by a single band at 3578/2644 cm^{-1}. The broad 3430 cm^{-1} band remains on heating, with a very weak OD equivalent, at ~2530 cm^{-1}. Heat treatment of NTAP4 (Ni-talc) at 500 °C for 1 h has very little effect on its spectrum (Fig. 5).

IR spectra of Ni-TAP: high-pressure results. In the diamond-anvil cell, the only bands that are strong enough to be resolved above 0 GPa are those at 3672 and 3626 cm^{-1} (OH) and 2676 cm^{-1} (OD) (Fig. 7). The 3256 cm^{-1} band is visible, but interference fringes prevent its position from being measured. On compression to 9.0 GPa, the 3626 and 2676 cm^{-1} bands show a small positive $d\nu/dP$, moving to 3628 cm^{-1} (OH) and 2679 cm^{-1} (OD). In

contrast, the 3672 cm^{-1} band shows a rapid decrease in frequency, shifting at a rate of -9 cm^{-1}/GPa over 3.5 GPa. At the same time, this band decreases in intensity so that by 5.3 GPa it can no longer be resolved. Both bands return to their original position on decompression.

DISCUSSION

Infrared band assignments

The main motivation for producing Ni-substituted TAP was to aid in assigning bands in IR spectra that previously have been the source of ambiguity. Substitution of 100% Ni for Mg in talc results in a well-documented wavenumber shift from 3676 to 3626 cm^{-1}, i.e., Ni for Mg causes a large (50 cm^{-1}) shift in OH vibrational frequency. If such shifts can be identified, then bands can be assigned to Mg/Ni-OH. Unshifted bands can then be assigned to H_2O or to Si-OH groups, which will be unaffected by Mg/Ni substitution as they are not bonded to Mg or Ni.

Band assignments are summarized in Table 2. In both the Mg-TAP and Ni-TAP spectra, there are sharp bands at the same frequencies as in Mg- and Ni-talc (highlighted by asterisks in Figs 4 and 5). These bands are assigned to Mg/Ni-OH/OD in the same environment as in talc. This is the same assignment as previously made (Parry et al. 2007; Pawley and Jones 2011). The intensity of this talc-like band is much lower in the DTAP3 single crystal spectrum (Fig. 4) than in the powder spectra. This is because the orientation of the single crystal was such that talc-like O-H bonds (parallel to [001]) would have been nearly parallel to the incident direction of the IR beam. In contrast, powder spectra are much more randomised and register all OH/OD bands.

If we compare the Mg-TAP and Ni-TAP spectra (Figs 4 and 5), we see that as well as the sharp talc-like band, the two pairs of OH bands at 3643/3630 and 3588/3577 cm^{-1} in the Mg-TAP spectra are related by 50 cm^{-1} shifts to the two OH bands at 3588 and 3532 cm^{-1}, respectively, in Ni-TAP. We identify these two sets of bands as being due to distinct Mg-OH/Ni-OH groups in TAP that are different from the talc-like OH group, and are, therefore, new OH environments that only occur in TAP. The model of TAP proposed by Phillips et al. (2007), and shown schematically in Figure 1, has three different Mg-OH environments. We propose that the sharp talc-like band corresponds to type-A OH, with the other two sets of bands being types B and C. The fine structure of the Mg-TAP spectra, in which these pairs of Mg-OH (and Mg-OD) bands are resolved as doublets, implies that these new Mg-OH (Mg-OD) environments are further subdivided by subtle interactions with the surrounding structure. The separate bands are not resolvable in the Ni-TAP spectra because the sample is not as well crystallized as the Mg-TAP samples. The bands at 3665 and 2704 cm^{-1} may also be doublets with the talc-like bands at 3675 and 2711 cm^{-1}. Their equivalents are not resolved in the Ni-TAP spectra.

Further indication that the 3675 cm^{-1} OH band in Mg-TAP (and equivalent OD and Ni-TAP bands) is due to OH in a talc-like environment comes from its behavior on compression. The small blue shift of the 3626 and 2676 cm^{-1} bands with compression of Ni-TAP is similar in direction and magnitude to the shift experienced by the 3675 and 2711 cm^{-1} bands in Mg-TAP (Pawley and Jones 2011), and by the 3676 cm^{-1} band in talc (e.g., Parry et al. 2007). The positive $d\nu/dP$ indicates that there is no hydrogen bonding, either to oxygens of the silica ring or to interlayer H_2O. $d\nu/dP$ is small because the 2:1 layers remain fairly rigid during compression, with most of the compression taken up by the interlayer

316 region. The persistence of the band in the spectra of DTAP4 heated to 500 and 600 °C is
317 further evidence of its being due to vibration of strongly bonded OH/OD. In contrast, the
318 interlayer water is driven off by 500 °C, as will be seen below. The invariance of the
319 vibrational frequency as the interlayer water is removed is a further indication of an
320 absence of hydrogen bonding between the talc-like OH and the interlayer H_2O.

321 The other band that is seen in the high-pressure Ni-TAP spectra, at ν_0 = 3672 cm^{-1},
322 experiences a large red shift on compression (Fig. 7). This behavior recalls that reported in
323 Mg-TAP by Parry et al. (2007). In their Figure 3, a broad band emerges from the 3675 cm^{-1}
324 band at ~1 GPa and moves to ~3640 cm^{-1} at 9.6 GPa. The behavior of these bands is similar
325 in Mg-TAP and Ni-TAP samples, and the two bands can, therefore, be confidently assigned
326 to the same stretching vibration. The similar values of ν_0 = 3672 cm^{-1} in Ni-TAP and ν_0 =
327 3675 cm^{-1} in Mg-TAP indicate that this band is not due to Mg/Ni-OH. The marked
328 wavenumber shift on compression suggests that it is associated with the interlayer region,
329 which has a high compressibility, rather than with the 2:1 layers. We therefore assign it to
330 stretching of one of the O-H bonds of the interlayer water. In previous studies its
331 assignment was uncertain (e.g., Pawley and Jones 2011), but comparison of Mg-TAP and Ni-
332 TAP spectra removes any ambiguity, and shows that the 3675 cm^{-1} band in Mg-TAP spectra
333 is a near coincidence of H_2O and talc-like Mg-OH bands. The negative $d\nu/dP$ of this H_2O
334 band suggests increasing hydrogen bonding as the interlayer H_2O is brought closer to the
335 neighbouring tetrahedral sheet.

336 Comparison of Figures 4 and 5 shows that the broad bands at 3268 and 2440 cm^{-1} in
337 the Mg-TAP spectra are equivalent to the 3256 and 2440 cm^{-1} bands in the Ni-TAP
338 spectrum. In this case there is only a small (OH), or no (OD), frequency shift with Mg-Ni

339 substitution. The bands can therefore be assigned to stretching of the other O-H/O-D bond
340 of the interlayer water. This is the same assignment as made by Parry et al. (2007). The
341 large bandwidth is interpreted as being due to a degree of orientational disorder. The low
342 frequency indicates stronger hydrogen bonding than for the other O-H/O-D bonds.

343 The presence of an OD band at 2731-2732 cm^{-1} in the spectra of both samples needs
344 further consideration. This band should have a corresponding OH band, but there are no
345 OH bands with frequency higher than 3675 cm^{-1}. However, it can be seen from Figure 4 that
346 the intensity of this band (highlighted with a vertical dashed line) varies between spectra
347 and roughly correlates with the intensity of the 2440 cm^{-1} band (also highlighted). These
348 two bands are particularly strong in the DTAP3 single crystal spectrum. Both bands are
349 weak in the Ni-TAP spectrum (Fig. 5). This correlation suggests that, like the 2440 cm^{-1}
350 band, the 2732 cm^{-1} band can be assigned to stretching of OD in interlayer water, and is
351 therefore the OD equivalent of the 3675 cm^{-1} interlayer H_2O band. That it has a different
352 ν_{OH}/ν_{OD} from the 3675 cm^{-1} talc-like Mg-OH band (1.345 versus 1.356) is puzzling, but it
353 should be noted that the lower-wavenumber H_2O band (3268 cm^{-1}) also has a low ν_{OH}/ν_{OD}
354 (1.339). The 2751 cm^{-1} shoulder on the 2732 cm^{-1} band in the Mg-TAP spectra has no
355 corresponding OH band, and remains an enigma.

356 The two bands assigned to OH/OD stretching of interlayer water are separated by
357 around 400 cm^{-1} (OH). This degree of separation indicates that the two vibrations are not
358 coupled, i.e. they are not symmetric and antisymmetric vibrations of H_2O. Instead, the two
359 O-H bonds can be considered separately and each has its own stretching frequency.
360 Assuming that in both Mg-TAP and Ni-TAP there are HOH, HOD and DOD molecules, the
361 absence of coupling is also evident from the fact that there are only two ν_{OH} and two ν_{OD} in

both spectra, since coupling would lead to two frequencies for each of the HOH, HOD and DOD molecules. The large frequency difference between the two bands indicates a significant difference in hydrogen bonding, with a much shorter O_w-H···O for the band at 3268 cm^{-1} than for the band at 3675 cm^{-1} (~ 2.7 Å compared with > 3.0 Å, using the correlation of Libowitzky 1999). This difference suggests that either the H_2O molecule does not occupy a symmetric position with respect to the adjacent SiO_4 tetrahedra, or that there is dynamic disorder between two non-symmetric positions, as is the case for lawsonite (Libowitzky and Rossman 1996). On compression there is a strengthening of the hydrogen bonding for the weakly hydrogen-bonded O-H; the other band is not resolved on compression.

It is curious that the OD bands of interlayer D_2O in Ni-TAP are much weaker than the corresponding OH bands. On the other hand, the talc-like OD band is relatively intense. This is seen even in the spectrum of the sample synthesized in < 1 h. Since the Ni-TAP samples were synthesized from $Ni_3Si_4O_{10}(OH)_2$ + D_2O, we might have expected the talc-like band to be stronger in the OH stretching region and the interlayer water bands to be stronger in the OD region. Instead, there appears to have been rapid exchange of the talc OH for OD, and preferential incorporation of H_2O in the interlayer.

All interlayer H_2O/D_2O bands in Mg-TAP and Ni-TAP spectra disappear after heating to 500 °C (Figs 5 and 6), an observation that is consistent with differential thermal analysis showing loss of interlayer water at around 450 °C at low pressure (Miller et al. 1991). Even after all the interlayer water has been removed, TAP still retains several structural differences from talc. The talc-like OH/OD band is the only band that is unchanged from the unheated spectra. The other bands are at different frequencies, indicating a structural

385 rearrangement, presumably caused by the removal of the interlayer H_2O. The new band
386 that appears as a shoulder on the high-frequency side of the main talc-like band shows the
387 same Mg-Ni frequency shift, indicating that it is also due to a Mg/Ni-OH/OD vibration. The
388 similar frequencies of the 3587/2651 cm^{-1} (Mg-TAP) and 3578/2644 cm^{-1} (Ni-TAP) bands
389 suggests that they include vibrations that are unaffected by Mg-Ni substitution, i.e.,
390 vibrations of silanol groups (see below). Their relative broadness suggests that they
391 comprise more than one overlapping band. The shoulder on the 2651 cm^{-1} band in the 500
392 °C DTAP4 spectra becomes resolved after heating at 600 °C into two bands at 2689 and
393 2677 cm^{-1}. The equivalent bands are too weak to be observed in the OH region.
394 The broad band at ~3430 cm^{-1} in both Mg-TAP and Ni-TAP specta is intriguing, as it is
395 of variable intensity, and appears to persist after heating, albeit with a small shift in
396 wavenumber. There is also a very weak OD equivalent, which is removed on heating Mg-
397 TAP to 600 °C. This band is in the region of the spectrum where adsorbed H_2O can be
398 expressed. We would expect much less adsorbed H_2O on single crystals than in powders,
399 and indeed, the band intensity is reduced in the single-crystal spectrum of DTAP3.
400 However, another possibility is that the band in the unheated samples' spectra is due to
401 additional H_2O in the interlayer. The NMR data of Phillips et al. (2007) suggest that as well
402 as the strongly hydrogen-bonded interlayer H_2O, there could be additional, more weakly
403 bonded interlayer H_2O, the amount of which could vary between samples. Variation of H_2O
404 content is also suggested by the variable estimates of water content obtained in previous
405 studies of TAP. We propose that the 3430 cm^{-1} peak is due to these more weakly-bonded
406 H_2O groups. These H_2O groups should be removed on heating to 500 °C, and so the

407 persistence of a feature at approximately the same wavenumber in the spectra of heated
408 samples is puzzling.
409
410 **Silanols?**
411 The structural model for TAP proposed by Welch et al. (2006) and Phillips et al.
412 (2007) has two important new features, both of which are associated with Si vacancies: (1)
413 two new Mg-OH environments; (2) silanol groups. The presence of silanols is considered
414 essential to providing hydrophilic character needed to incorporate interlayer H_2O, and
415 stands in sharp contrast to the hydrophobic nature of talc. In the study reported here, we
416 have identified three distinct Mg-OH (Ni-OH) environments in TAP, two of which appear to
417 be unique to TAP. These two new Mg-OH sites may be further subdivided into pairs arising
418 from more subtle interactions with the surrounding structure. However, we have not
419 identified silanol groups spectroscopically. A search of the very limited literature on
420 silanols in silicate minerals indicates that silanol vibrations occur over a wide wavenumber
421 range from 3000 – 3700 cm^{-1}. It is possible that the 3587 cm^{-1} (Mg-TAP) and 3578 cm^{-1} (Ni-
422 TAP) bands in the heated spectra are due to silanol groups, as their frequency is almost the
423 same for both samples. Bands at these frequencies do not occur in the unheated samples'
424 spectra; however, we would not expect them to, since hydrogen bonding to the interlayer
425 H_2O would cause a reduction in frequency. It may be that the silanol bands are not visible
426 because they overlap with the low-frequency H_2O bands.
427

Reproducibility of TAP structure

The similarity of IR spectra and unit-cell parameters of samples of TAP synthesized under widely varying run durations (150 – 400 h for Mg-TAP, < 1 – 97 h for Ni-TAP) shows that the key features of their structural states are reproducible. Likewise, Ni-TAP is a good analogue of Mg-TAP, there being a close correspondence between their spectra and an analogous response to compression. If there is any variability, it is in the extent of weakly-bonded interlayer H_2O whose presence is implied by the broad spectral feature at ~3430 cm^{-1}.

The 3T superstructure

The presence of a 3*T* superlattice in DTAP3 points to a further level of structural complexity beyond that of the monoclinic substructure reported by Comodi et al. (2005). The DTAP3 diffraction patterns are very similar to those of 3*T* phengite (Schingaro et al. 2013), except for the presence of significant modulated non-Bragg intensity in the former. This similarity suggests that interlayer H_2O positions in TAP correlate with those of K in phengite. It may be possible to determine the crystal structure of this 3T polytype using radiation with a wavelength longer than that of MoKα, for example CuKα. We are exploring this possibility.

IMPLICATIONS

The complexity of the IR spectra of Mg-TAP and Ni-TAP is evidence for a structural modification of the talc-like 2:1 layer building block of 10-Å phase that stabilizes the incorporation of interlayer H_2O. Following Phillips et al. (2007), we propose that Si

vacancies and silanol groups are formed when talc transforms to 10-Å phase, making the 2:1 layer hydrophilic and enabling the incorporation of interlayer H_2O. The presence of silanol groups means that 10-Å phase can incorporate more water than proposed for structural models in which water is only present as interlayer H_2O. It also means that if another phyllosilicate shows solid solution or lamellar intergrowths with 10-Å phase at high pressure, such as has been proposed for phlogopite (Fumagalli et al. 2009), it too is likely to contain silanol groups.

The reproducibility in detail of the main structural features of 10-Å phase implies that the concentration of Si vacancies and silanol groups is essentially constant. A well-defined H_2O content may imply ordered arrangement of Si vacancies and silanol groups, in turn producing an ordered arrangement of interlayer H_2O that defines a characteristic stoichiometry. The presence of a 3*T*-superstructure may be associated with such ordering. An ordered structure means that any variation in measured H_2O content of 10-Å phase samples is likely to be due to weakly bonded interlayer H_2O. This H_2O is assumed to be incorporated during quenching and decompression, as inferred from phase equilibrium experiments on two apparently different samples of 10-Å phase, which suggested no difference in water content at high pressures and temperatures (Pawley et al. 2011). Therefore, in the Earth's mantle, 10-Å phase should have a fixed composition and H_2O content.

ACKNOWLEDGEMENTS

ARP would like to thank Ray Jones of CCLRC for help with IR data collection at Daresbury Laboratory. MDW would like to thank Dr Philippe Lerch of the Swiss Light Source synchrotron radiation laboratory, Villigen, Switzerland, for technical advice and for

making his IR laboratory equipment available for the high-pressure experiment on Ni-TAP. MDW acknowledges support of his research on hydrous minerals from The Natural History Museum (London). We thank Monika Koch-Müller and Sabrina Nazzareni for their comments on the manuscript.

REFERENCES CITED

Bauer, J.F. and Sclar, C.B. (1981) The "10Å phase" in the system MgO-SiO_2-H_2O. American Mineralogist, 66, 576-585.

Comodi, P., Fumagalli, P., Nazzareni, S., and Zanazzi, P.F. (2005) The 10 Å phase: Crystal structure from single-crystal X-ray data. American Mineralogist, 90, 1012-1016.

Evans, B.W. and Guggenheim, S. (1988) Talc, pyrophyllite, and related minerals. In S.W. Bailey, Eds., Hydrous phyllosilicates (exclusive of micas), Reviews in Mineralogy, Vol 19, p. 225-294. Mineralogical Society of America, Washington, D.C.

Farrugia, L.J. (1999) WinGX suite for small-molecule single-crystal crystallography. Journal of Applied Crystallography, 32, 837-838.

Fumagalli, P. and Stixrude, L. (2007) The 10 Å phase at high pressure by first principles calculations and implications for the petrology of subduction zones. Earth and Planetary Science Letters, 260, 212-226.

Fumagalli, P., Zanchetta, S., and Poli, S. (2009) Alkali in phlogopite and amphibole and their effects on phase relations in metasomatized peridotites: a high-pressure study. Contributions to Mineralogy and Petrology, 158, 723-737.

Hirauchi, K., den Hartog, S.A.M., and Spiers, C.J. (2013) Weakening of the slab-mantle wedge interface induced by metasomatic growth of talc. Geology, 41, 75-78.

Jennings, E. S., Montgomery, W., and Lerch, Ph. (2010) The stability of coronene at high temperature and pressure: implications for hydrocarbons in planetary interiors. Journal of Physical Chemistry B, 114, 15753–15758.

Libowitzky, E. (1999) Correlation of O-H stretching frequencies and O-H□□□O hydrogen bond lengths in minerals. Monatshefte Fur Chemie, 130, 1047-1059.

Libowitzky, E. and Rossman, G.R. (1996) FTIR spectroscopy of lawsonite between 82 and 325 K. American Mineralogist, 81, 1080-1091.

Mao, H.K., Xu, J., and Bell, P.M. (1986) Calibration of the ruby pressure scale to 800-kbar under quasi-hydrostatic conditions. Journal of Geophysical Research-Solid Earth and Planets, 91, 4673-4676.

Miller, A.K., Guggenheim, S., and Koster van Groos, A.F. (1991) The incorporation of "water" in a high-pressure 2:1 layer silicate: A high pressure differential thermal analysis of the 10 Å phase. American Mineralogist, 76, 106-112.

Parry, S.A., Pawley, A.R., Jones, R.L., and Clark, S.M. (2007) An infrared spectroscopic study of the OH stretching frequencies of talc and 10-Å phase to 10 GPa. American Mineralogist, 92, 525-531.

Pawley, A. and Jones, R. (2011) Hydroxyl stretching in phyllosilicates at high pressures and temperatures: an infrared spectroscopic study. Physics and Chemistry of Minerals, 38, 753-765.

Pawley, A.R. and Wood, B.J. (1995) The high-pressure stability of talc and 10 Å phase: potential storage sites for H_2O in subduction zones. American Mineralogist, 80, 998-1003.

519 Pawley, A., Chinnery, N., Clark, S., and Walter, M. (2011) Experimental study of the
520 dehydration of 10-Å phase, with implications for its H_2O content and stability in
521 subducted lithosphere. Contributions to Mineralogy and Petrology, 162, 1279-1289.
522 Phillips, B.L., Mason, H.E., and Guggenheim, S. (2007) Hydrogen bonded silanols in the 10 Å
523 phase: Evidence from NMR spectroscopy. American Mineralogist, 92, 1474-1485.
524 Sclar, C.B., Carrison, L.C., and Schwartz, C.M. (1965) High pressure synthesis and stability of
525 a new hydronium bearing layer silicate in the system MgO-SiO_2-H_2O. Eos, 46, 184.
526 Schingaro, E., Lacalamita, M., Scordari, F., and Mesto, E. (2013) 3T-phengite from Kasenyi
527 kamafugite (SW Uganda): EPMA, XPS, FTIR, and SCXRD study. American
528 Mineralogist, 98, 709-717.
529 Sheldrick, G.M. (2008) A short history of SHELX. Acta Crystallographica, A64, 112-122.
530 Welch, M.D., Pawley, A.R., Ashbrook, S.E., Mason, H.E., and Phillips, B.L. (2006) Si vacancies
531 in the 10-Å phase. American Mineralogist, 91, 1707-1710.
532 Welch, M.D., Montgomery, W., Balan, E., and Lerch, P. (2012) Insights into the high-pressure
533 behaviour of kaolinite from infrared spectroscopy and quantum-mechanical
534 calculations. Physics and Chemistry of Minerals, 39, 143-151.
535 Wunder, B. and Schreyer, W. (1992) Metastability of the 10-Å phase in the system MgO-
536 SiO_2-H_2O (MSH). What about hydrous MSH phases in subduction zones? Journal of
537 Petrology, 33, 877-889.
538 Yamamoto, K. and Akimoto, S. (1977) The system MgO-SiO_2-H_2O at high pressures and
539 temperatures — stability field for hydroxyl-chondrodite, hydroxyl-clinohumite and
540 10 Å-phase. American Journal of Science, 277, 288-312.
541

Table 1. Synthesis conditions and run products of Ni-TAP (this study) and Mg-TAP (Welch et al. 2006). Abbreviations: TAP = 10-Å phase, amph = amphibole, en = clino-enstatite.

Experiment	Starting material	Pressure (GPa)	Temperature (°C)	Duration (h)	Run product	Fluid in excess?
NTAP1	Ni-talc+D_2O	6.5	600	0.7	TAP	yes
NTAP2	Ni-talc +D_2O	6.5	600	6	TAP	yes
NTAP3	Oxide gel+D_2O	6.2	600	100	talc + amph	no
NTAP4	Ni-talc +D_2O	6.2	600	48	talc (+ TAP)	yes
NTAP5	Ni-talc +D_2O	7.0	600	97	TAP	yes
DTAP3	$Mg(OD)_2$ + SiO_2	6.5	600	400	TAP	yes
DTAP4	$Mg(OD)_2$ + SiO_2	6.5	600	150	TAP (+ en)	yes

Table 2. Summary of OH and OD stretching frequencies and their assignments for Mg-TAP, Ni-TAP and samples heated at 500 °C for 1 – 2 h. Figures in parentheses are the pressure dependence (cm^{-1}/GPa) for the strongest Ni-TAP bands, measured up to 9 GPa (3626 and 2676 cm^{-1} bands) and up to 3.5 GPa (3672 cm^{-1} band). Assignments described as "New Mg-OH" are Mg/Ni-OH/OD environments that are not present in talc.

ν_{OH} (cm^{-1})	ν_{OD} (cm^{-1})	ν_{OH} (cm^{-1})	ν_{OD} (cm^{-1})	Assignment
Mg-TAP		Ni-TAP		
3268	2440	3256	2440	Interlayer H_2O
3430	2555	3430	-	Weakly bonded H_2O?
3577	2626	3532	2607	New Mg-OH
3588	2645			
3630	2668	3588	2648	New Mg-OH
3643	2683			
3665	2704			
3675	2711	3626 (0.2)	2676 (0.3)	Talc-like Mg-OH
3675	2732	3672 (-9)	2731	Interlayer H_2O
Heated Mg-TAP		Heated Ni-TAP		
3445	2530	3430	2530	Weakly bonded H_2O?
3587	2651	3578	2644	Silanol?
3675	2711	3626	2676	Talc-like Mg-OH
3686	2719	3637	2684	New Mg-OH

Figure captions

Figure 1. The 2:1 layer OH sites in TAP based upon the model proposed by Phillips et al. (2007). The structure of a 2:1 layer is shown projected onto (001) with $^{[6]}$Mg octahedra (yellow), SiO_4 tetrahedra (blue), O and H atoms (grey and teal-green, respectively) of OH and H_2O groups. Other O atoms are omitted for clarity. Three different OH environments labelled A, B and C are shown. A sites are normal talc-like OH; B and C sites are new OH groups that arise from the presence of Si vacancies in the sheet of tetrahedra. One such Si vacancy and its associated OH groups is shown.

Figure 2. X-ray diffraction patterns of Ni-TAP (sample NTAP1) and Ni-talc (sample NTAP4). The bands marked with asterisks are the (001), (003) and (004) basal spacing reflections.

Figure 3. (a) An a^*-c^* diffraction pattern of TAP indexed for the 3T supercell (trigonal) and showing the rows of superlattice reflections that occur for h, $k \neq 3n$, as is also seen in 3T phengite (Schingaro et al. 2013). (b) Two-dimensional diffraction profile along part of the 10l row of superlattice reflections indicated by the area in (a) defined by the dashed box. Although most peaks are easily located, the considerable peak overlap prevented successful integration of intensity.

Figure 4. IR spectra of Mg-TAP in the OH and OD stretching regions. The DTAP3 spectra were collected at Daresbury Laboratory, the DTAP4 spectrum at the Natural History Museum. The region of the spectra between 2800 and 3050 cm^{-1} contains vibrations of

624 organic compounds which have been omitted for clarity. Vertical dashed lines = positions
625 of the stretching vibrations of the interlayer H_2O/D_2O, * = talc-like OH/OD stretching
626 vibrations (only shown above the top spectrum). See text for further discussion.
627
628 **Figure 5.** IR spectra of Ni-TAP and Ni-talc in the OH and OD stretching regions. The talc
629 sample contains a small amount of TAP. Also shown are spectra of Ni-TAP and Ni-talc
630 heated at 500 °C for 1 hour. The dashed lines and asterisks represent the same features as
631 in Figure 4.
632
633 **Figure 6.** IR spectra of Mg-TAP in the OH and OD stretching regions after heating at 500
634 and 600 °C. The spectra represent three separate heating experiments. Also shown is the
635 unheated spectrum of disc 1. The dashed lines and asterisks represent the same features as
636 in Figure 4.
637
638 **Figure 7.** IR spectra of Ni-TAP (NTAP1) under compression in the diamond-anvil cell. The
639 upper three spectra were collected during decompression.

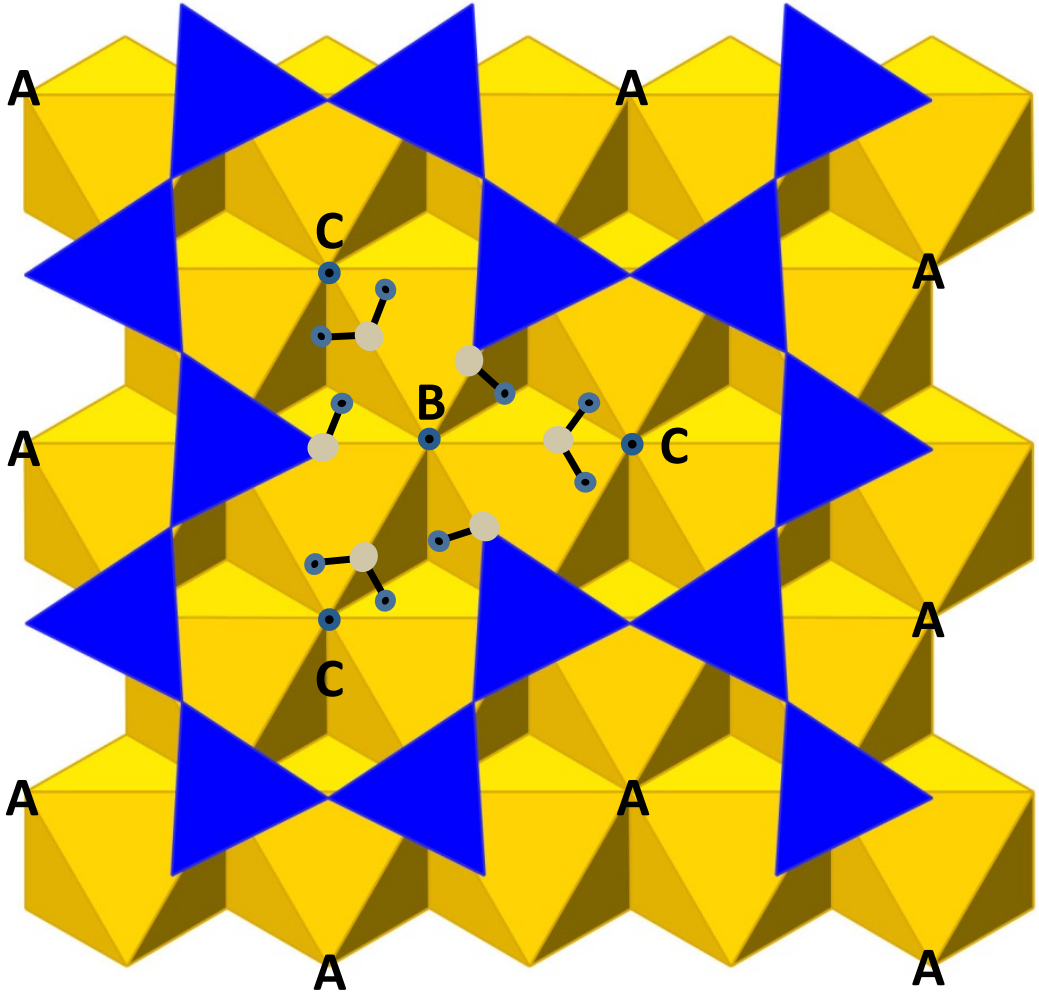
A
A
C
A
B
A
C
C
A
A
A
A

Ni-TAP

Ni-talc

Intensity

2 theta (deg)

10 15 20 25 30 35 40

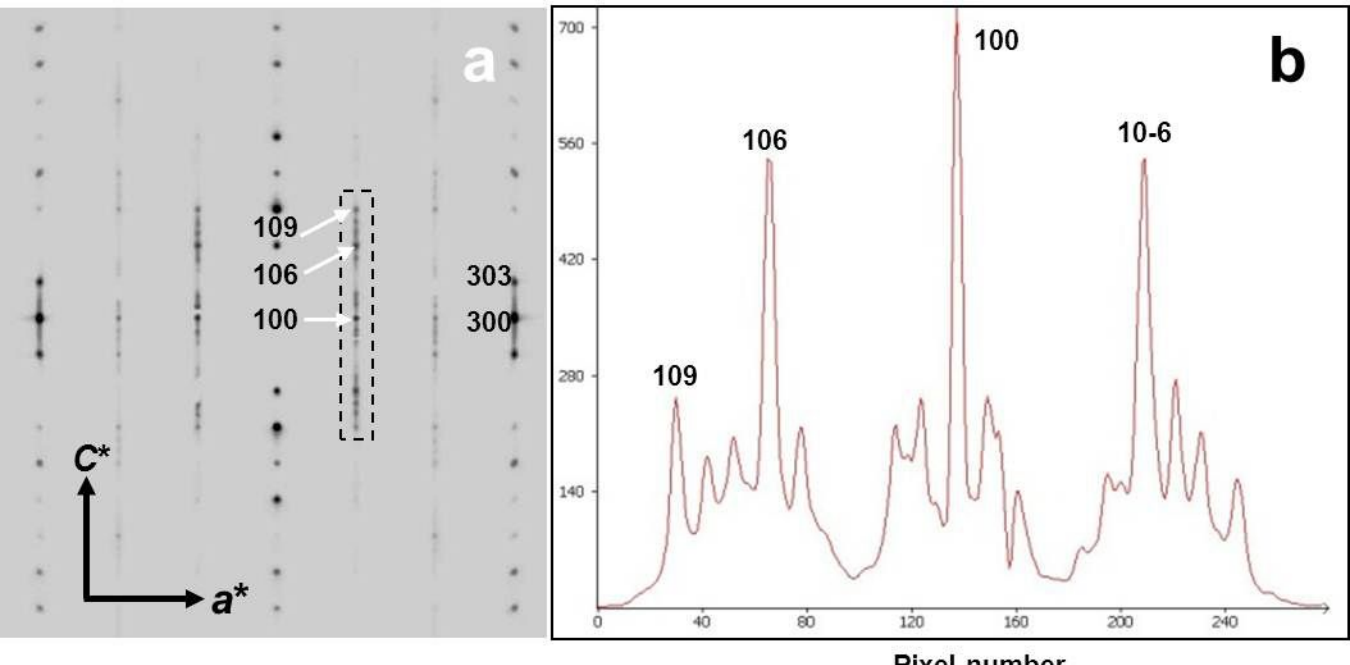
a
109
106
100
303
300
C*
a*
b
700
560
420
280
140
0
40
80
120
160
200
240
100
106
10-6
109
Pixel number

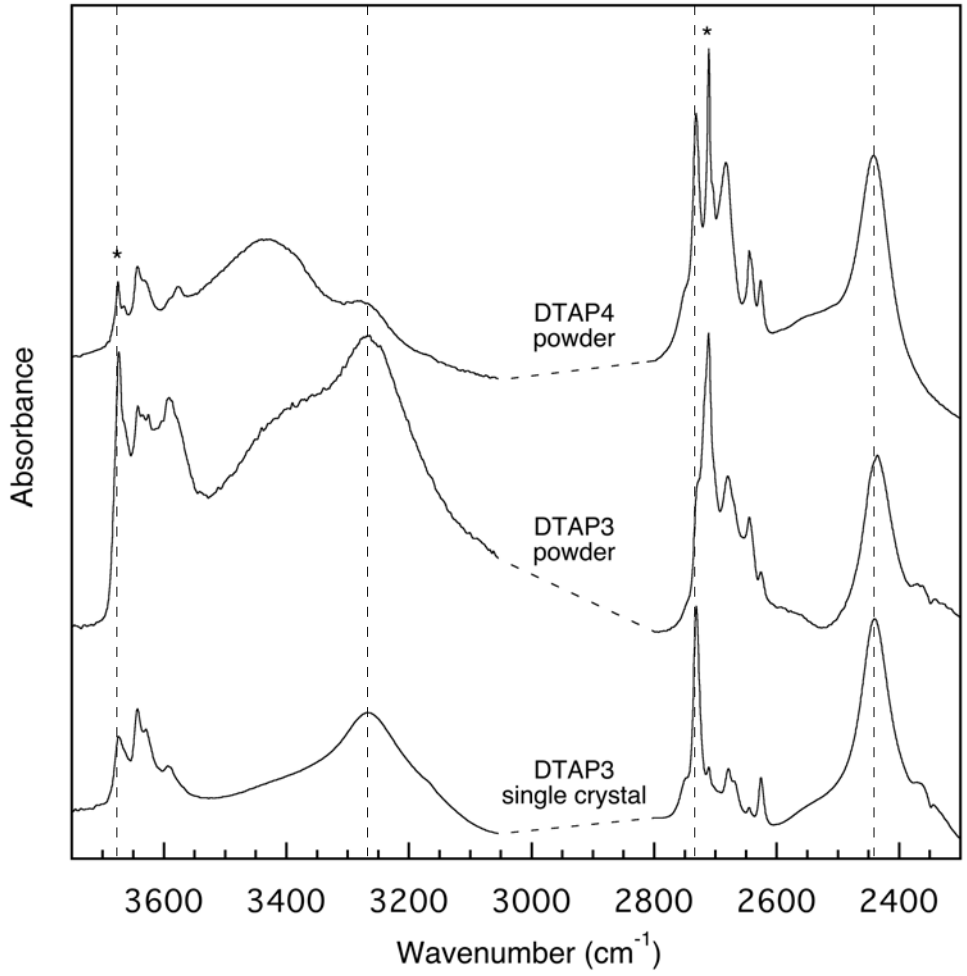
Absorbance
DTAP4
powder
DTAP3
powder
DTAP3
single crystal
*
*
3600
3400
3200
3000
2800
2600
2400
Wavenumber (cm-1)

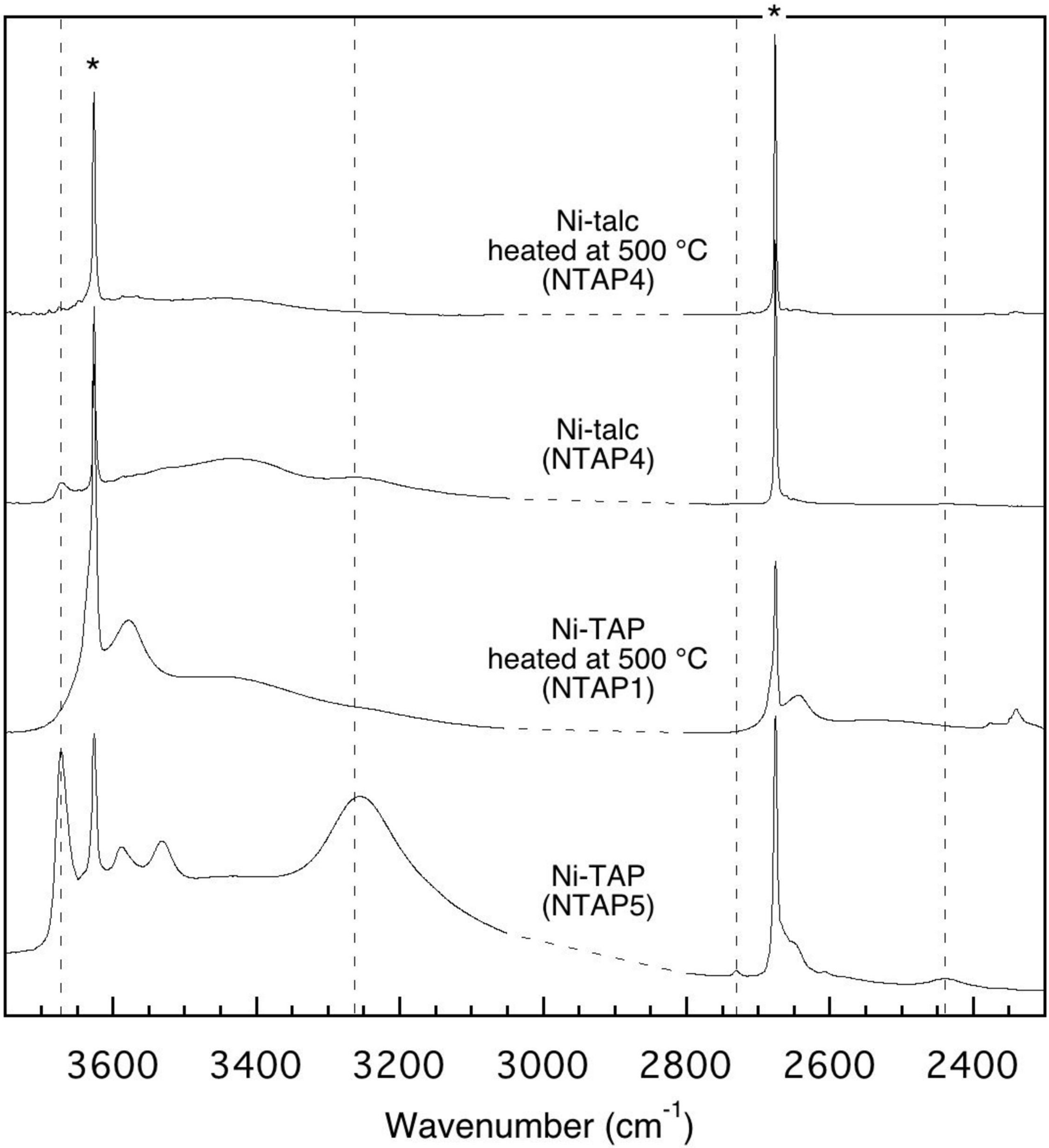
*
*
Ni-talc
heated at 500 °C
(NTAP4)
Ni-talc
(NTAP4)
Ni-TAP
heated at 500 °C
(NTAP1)
Ni-TAP
(NTAP5)
Absorbance
3600
3400
3200
3000
2800
2600
2400
Wavenumber (cm-1)

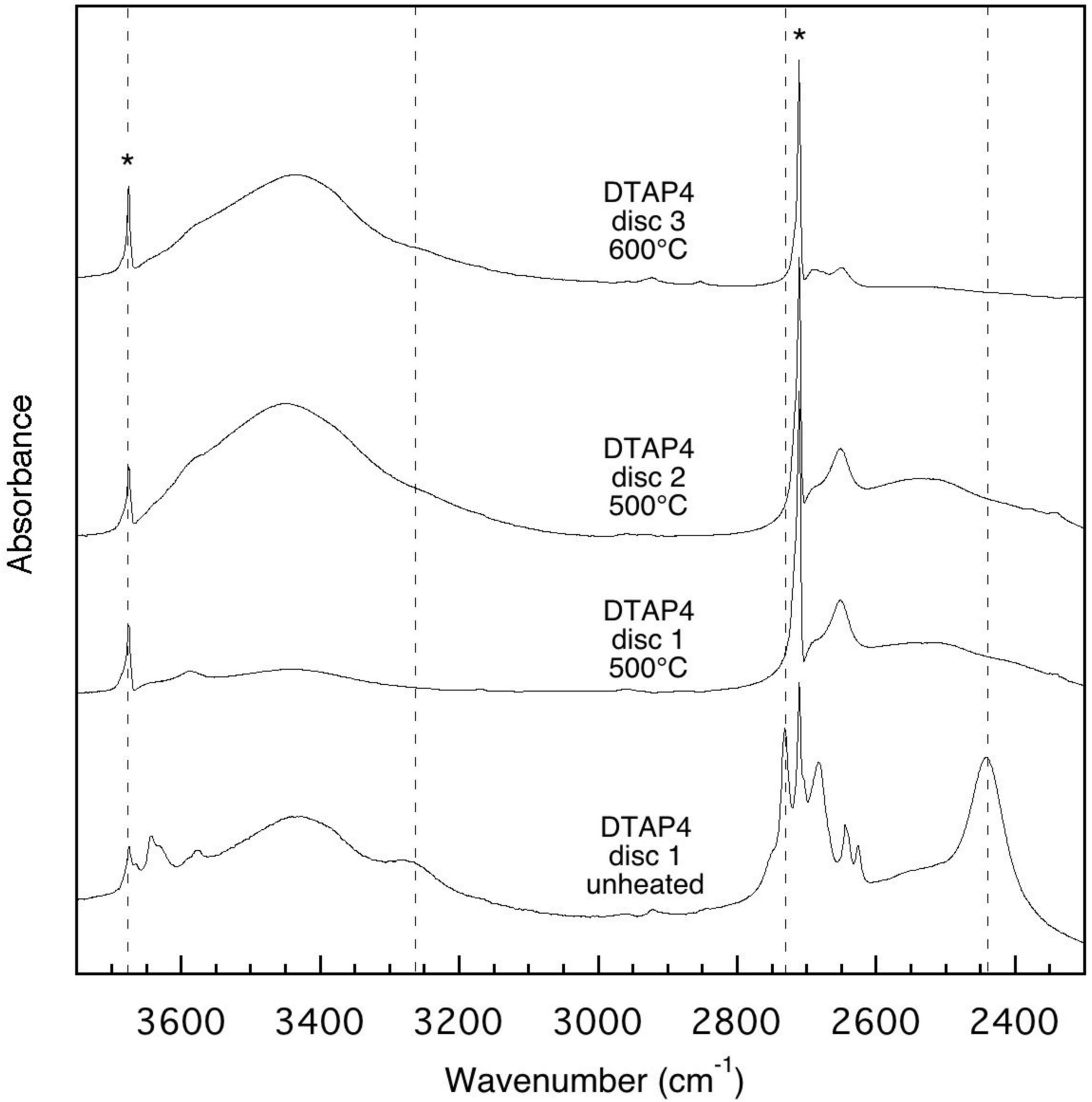
*
*
DTAP4
disc 3
600°C
DTAP4
disc 2
500°C
DTAP4
disc 1
500°C
DTAP4
disc 1
unheated
Absorbance
3600
3400
3200
3000
2800
2600
2400
Wavenumber (cm-1)

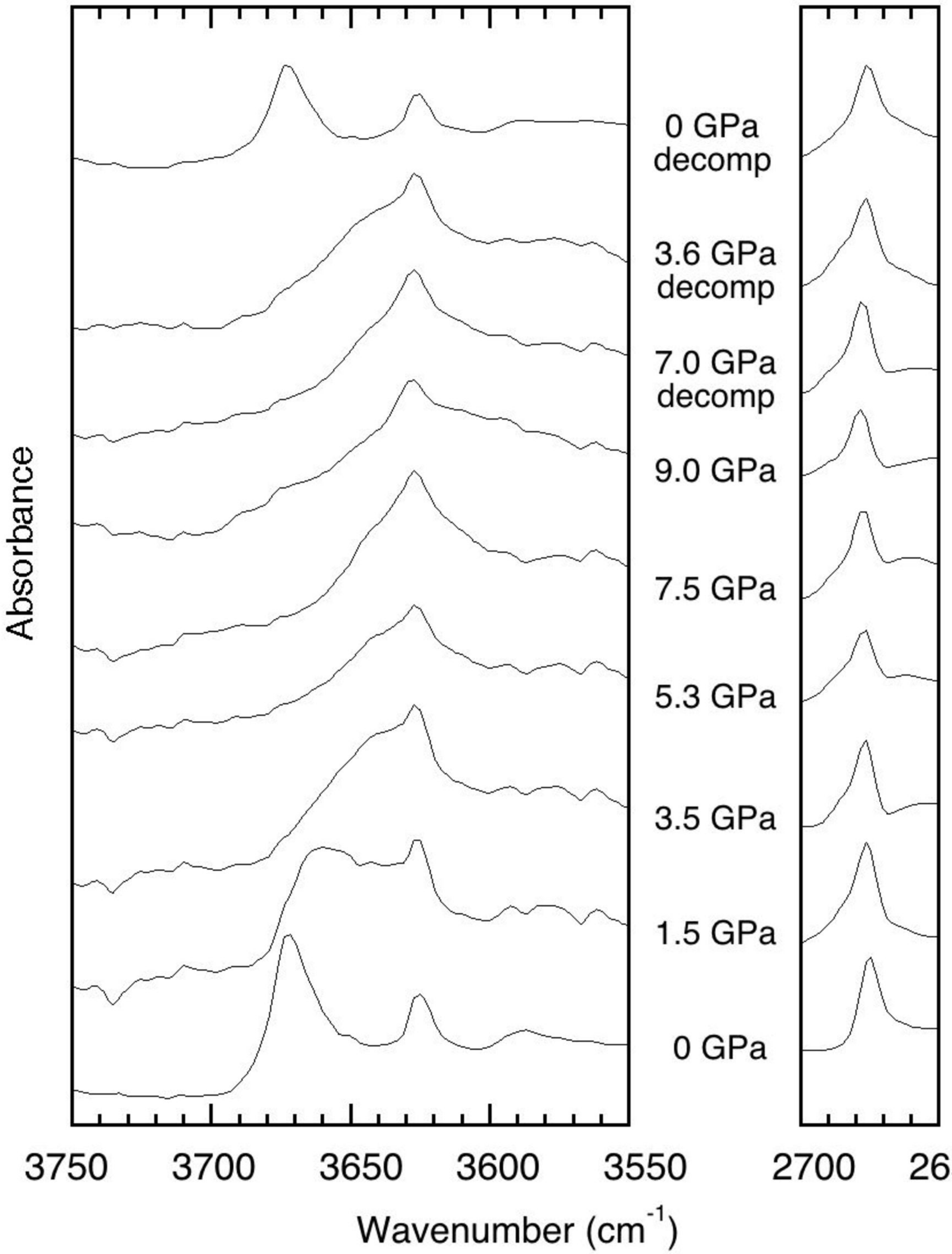
0 GPa
decomp
3.6 GPa
decomp
7.0 GPa
decomp
9.0 GPa
7.5 GPa
5.3 GPa
3.5 GPa
1.5 GPa
0 GPa
Absorbance
3750
3700
3650
3600
3550
2700
2650
Wavenumber (cm-1)